BRAIN COMMUNICATIONS

Neuroanatomical spread of amyloid β and tau in Alzheimer's disease: implications for primary prevention

Philip S. Insel,[1,2] Elizabeth C. Mormino,[3] Paul S. Aisen,[4] Wesley K. Thompson[5] and Michael C. Donohue[4]

With recent advances in our understanding of the continuous pathophysiological changes that begin many years prior to symptom onset, it is now apparent that Alzheimer's disease cannot be adequately described by discrete clinical stages, but should also incorporate the continuum of biological changes that precede and underlie the clinical representation of the disease. By jointly considering longitudinal changes of all available biomarkers and clinical assessments, variation within individuals can be integrated into a single continuous measure of disease progression and used to identify the earliest pathophysiological changes. Disease time, a measure of disease severity, was estimated using a Bayesian latent time joint mixed-effects model applied to an array of imaging, biomarker and neuropsychological data. Trajectories of regional amyloid β and tau PET uptake were estimated as a function of disease time. Regions with early signs of elevated amyloid β uptake were used to form an early, focal composite and compared to a commonly used global composite, in a separate validation sample. Disease time was estimated in 279 participants (183 cognitively unimpaired individuals, 61 mild cognitive impairment and 35 Alzheimer's disease dementia patients) with available amyloid β and tau PET data. Amyloid β PET uptake levels in the posterior cingulate and precuneus start high and immediately increase with small increases of disease time. Early elevation in tau PET uptake was found in the inferior temporal lobe, amygdala, banks of the superior temporal sulcus, entorhinal cortex, middle temporal lobe, inferior parietal lobe and the fusiform gyrus. In a separate validation sample of 188 cognitively unimpaired individuals, the early, focal amyloid β PET composite showed a 120% increase in the accumulation rate of amyloid β compared to the global composite ($P < 0.001$), resulting in a 60% increase in the power to detect a treatment effect in a primary prevention trial design. Ordering participants on a continuous disease time scale facilitates the inspection of the earliest signs of amyloid β and tau pathology. To detect early changes in amyloid β pathology, focusing on the earliest sites of amyloid β accumulation results in more powerful and efficient study designs in early Alzheimer's disease. Targeted composites could be used to re-examine the thresholds for amyloid β-related study inclusion, especially as the field shifts to focus on primary and secondary prevention. Clinical trials of anti-amyloid β treatments may benefit from the use of focal composites when estimating drug effects on amyloid β and tau changes in populations with minimal amyloid β and tau pathology and limited expected short-term accumulation.

1 Department of Psychiatry, University of California, San Francisco, CA, USA
2 Clinical Memory Research Unit, Department of Clinical Sciences Malmö, Lund University, Sweden
3 Department of Neurology and Neurological Sciences, Stanford University, Stanford, CA, USA
4 Alzheimer's Therapeutic Research Institute, Keck School of Medicine, University of Southern California, San Diego, CA, USA
5 Department of Family Medicine and Public Health, University of California, San Diego, CA, USA

Correspondence to: Philip S. Insel
Department of Psychiatry,
University of California, San Francisco, CA, USA
E-mail: philipinsel@ucsf.edu

Received December 9, 2019. Revised December 11, 2019. Accepted December 16, 2019. Advance Access publication February 6, 2020

Keywords: amyloid β; tau; Alzheimer's disease; primary prevention

Abbreviations: Aβ = amyloid β; AD = Alzheimer's disease; ADAS-cog = Alzheimer's disease assessment scale, cognitive subscale; ADNI = Alzheimer's Disease Neuroimaging Initiative; AIC = Akaike information criterion; *APOE* = Apolipoprotein E; BSTS = banks of the superior temporal sulcus; CDR = clinical dementia rating; CI = confidence interval; CU = cognitively unimpaired; EMCI = early mild cognitive impairment; LMCI = late mild cognitive impairment; LTJMM = latent time joint mixed-effects model; LTL = lateral temporal lobe; MCI = mild cognitive impairment; MMSE = mini-mental state exam; MTL = medial temporal lobe; pCU = cognitively unimpaired to mild cognitive impairment progressors; pMCI = mild cognitive impairment to Alzheimer's disease progressors; ROI = region of interest

Graphical Abstract

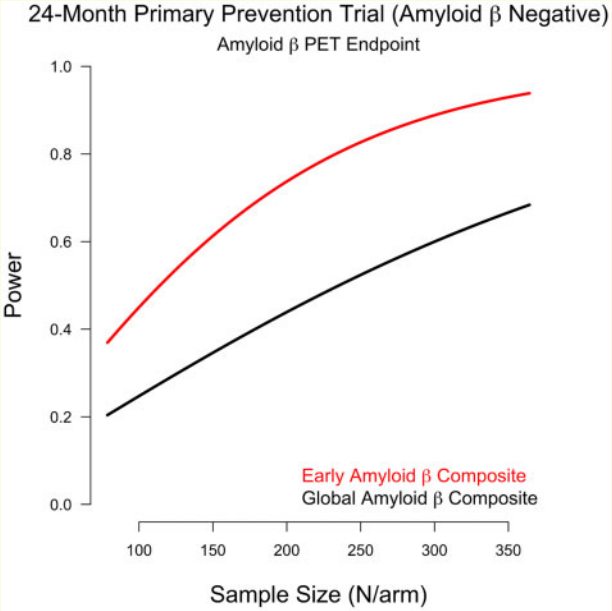

Introduction

Traditionally, Alzheimer's disease (AD) has been primarily described in terms of discrete clinical stages. However, with recent advances in our understanding of the continuous pathophysiological changes that begin many years prior to symptom onset, it is now apparent that AD cannot be adequately described by clinical stages, but should also incorporate the continuum of biological changes that precede and underlie the clinical representation of the disease (Aisen *et al.*, 2017). Conceptualizing the progression of AD as a continuum of overlapping pathological and subsequent clinical changes will facilitate a realistic examination of the time course of the disease. Clarifying this time course, from initial biomarker changes to severe functional impairment, is essential for accurate early diagnosis, clinical trial enrollment, disease monitoring and eventual disease prevention and management.

The likelihood of successfully treating AD may be highest in the earliest stages of the disease, requiring a detailed understanding of incipient biomarker changes. Considerable evidence confirms the accumulation of fibrillar amyloid β (Aβ) and aggregates of hyperphosphorylated tau, the pathognomonic lesions, as early AD biomarker changes. In this study, we focus on the early development of Aβ and tau pathology in order to provide finer detail about the temporal course of early neuropathological changes in AD. By jointly considering longitudinal changes of an array of neuropsychological, imaging and biomarker data, the variation within individuals and the associations among multiple outcomes are simultaneously integrated into a single continuous measure of disease progression (Donohue *et al.*, 2014; Li *et al.*, 2017, 2018). Using estimates of each participant's location on the disease continuum, or 'disease time', we sought to estimate a temporal ordering of spatial changes of Aβ and tau lesions throughout the brain. After identifying the earliest regions to demonstrate pathological changes, we tested the performance of these early regions in hypothetical primary and secondary prevention clinical trial settings in a separate validation sample.

Materials and methods

Participants

Data were obtained from the Alzheimer's Disease Neuroimaging Initiative (ADNI) database (adni.loni.usc.edu, www.adni-info.org). This study was approved by the Institutional Review Boards of all of the participating institutions. Informed written consent was obtained from all participants at each site. The population in this study included ADNI participants with measurements of both Aβ and tau PET. All available participants who were cognitively unimpaired (CU), Aβ+ mild cognitive impairment (MCI) or Aβ+ AD dementia at baseline were included, where Aβ+ was defined using a previously established threshold (SUVR = 1.10) (Joshi *et al.*, 2012). Impaired Aβ− participants were excluded due to impairment ostensibly unrelated to AD.

A separate validation sample included CU ADNI participants with measurements of Aβ who were not included in the first part of the analysis because of missing tau PET information.

PET imaging and CSF Aβ

Methods to acquire and process Aβ (18F-florbetapir) PET image data were described previously (Landau *et al.*, 2012). Twenty Aβ PET region of interests (ROIs) were analysed: the inferior, middle and superior temporal lobe; the precuneus, supramarginal gyrus, inferior and superior parietal lobe; the isthmus, posterior, caudal and rostral anterior cingulate; and the pars opercularis, pars triangularis, pars orbitalis, caudal and rostral middle frontal, medial and lateral orbitofrontal, frontal pole and superior frontal lobe.

Methods to acquire and process tau (18F-flortaucipir) PET image data were described previously (Maass *et al.*, 2017). Thirty tau ROIs were analysed: the amygdala, entorhinal cortex, parahippocampus, fusiform, banks of the superior temporal sulcus (BSTS), transverse temporal lobe, temporal pole, and the inferior, middle and superior temporal lobe; the isthmus cingulate, precuneus, supramarginal gyrus, and the inferior and superior parietal lobe; the pars orbitalis, pars triangularis, pars opercularis, lateral and medial orbitofrontal, pre- and paracentral, rostral, caudal, middle and superior frontal lobe; and the cuneus, lingual, pericalcarine, and lateral occipital lobe. Full details of PET acquisition and analysis can be found at http://adni.loni.usc.edu/methods/.

CSF samples were analysed for CSF Aβ42 using the AlzBio3 assay (Fujirebio, Ghent, Belgium) on the xMAP Luminex platform and have been described previously (Olsson *et al.*, 2005; Shaw *et al.*, 2009). CSF Aβ <192 ng/L defined CSF Aβ+.

Statistical analysis

Continuous disease time, an alternative to discrete diagnostic categories, as described and estimated previously (Donohue *et al.*, 2014; Li *et al.*, 2017, 2018) was used to model the spread of regional uptake in Aβ and tau PET (not used in the estimation of disease time). Disease time is a measure of disease severity, estimated from a Bayesian latent time joint-mixed effects model (LTJMM). Briefly, for subject i ($i=1, \ldots, n$), outcome k ($k=1, \ldots, p$), at time $t[ijk]$ ($j=1, \ldots, q_{ik}$) the model is of the form:

$$y_{ijk} = \mathbf{x}'_{t[ijk]}\boldsymbol{\beta}_k + \gamma_k(t[ijk] + \delta_i) + \alpha_{0ik} + \alpha_{1ik}t[ijk] + \varepsilon_{ijk},$$

where y_{ijk} are the observed outcome, $\mathbf{x}'_{t[ijk]}$ are vectors of predictors, $\boldsymbol{\beta}_k$ are fixed effects, γ_k are the disease time slopes, $t[ijk] + \delta_i$ are the shifted disease times, α are random effects and ε are multivariate Gaussian residuals. Jointly modeled outcomes included cognitive data (the 13-item Alzheimer's disease assessment scale, cognitive subscale, the mini-mental state exam, the Functional Activities Questionnaire, the Rey Auditory Visual Learning Test, the CDR Sum of Boxes and the Preclinical Alzheimer Cognitive Composite), CSF data (Aβ, phosphorylated tau and total tau), MRI volumes (hippocampus, entorhinal cortex, fusiform, middle temporal gyrus, ventricles and whole-brain volume) and PET imaging of global amyloid burden and glucose metabolism in the brain. LTJMM provides estimates of disease severity while accounting for the dependency between different markers. Prior to modeling, outcomes are transformed to quantiles, then transformed again to Z-scores via the inverse Gaussian cumulative distribution function. See Li *et al.* (2018) for more detail.

The relationship between longitudinal uptake in PET ROIs and disease time was examined using mixed-effects models with random intercepts. Natural splines were used to capture departures from linearity with respect to disease time. Spline knots were placed at the median and boundaries of disease time, with the number of knots selected by Akaike information criterion. PET responses were covaried for age, sex and mean Aβ PET uptake in the whole cerebellum for Aβ ROIs and mean tau PET uptake in the inferior cerebellar grey matter for tau ROIs.

We used a positional variance diagram to depict the temporal ordering of the ROIs. For a specific point on the disease time axis, ROIs were ordered by PET uptake. The positional variance diagram shows the proportion of 500 bootstrap samples in which a particular ROI appears in a particular position in the central ordering. Positional variance was assessed 15, 10 and 5 years before the estimated time of AD dementia diagnosis.

To further inspect early development of Aβ and tau pathology, changes in mean uptake with small increases in disease time (first derivatives of uptake curves) were plotted to show how the regional slopes of accumulation accelerate over disease time. Aβ regions with high mean

uptake early on the spectrum of disease time and continued increase with advances in disease time were evaluated further in the validation sample. Baseline and longitudinal change in a composite of regions with early uptake were compared to a commonly used global composite (comprising regions throughout the frontal, parietal and temporal lobes and cingulate gyrus; Landau *et al.*, 2012) in a sample of CSF Aβ− CU participants, and separately, CSF Aβ+ CU participants. Baseline and accumulation rate differences between early and global estimates were tested using *t*-tests with bootstrap estimated standard errors.

To estimate power for Aβ PET end-points in hypothetical primary and secondary prevention trials, mixed-model estimates were used to calculate the power for 24-month clinical trials, assuming a range of sample sizes, a 100% slowing of Aβ accumulation, a 12-month visit interval and a 30% dropout rate.

Associations between diagnosis and demographics were assessed using Wilcoxon rank-sum test for continuous variables and Fisher's Exact test for categorical variables. All analyses were done in R v3.5.1 (www.r-project.org).

Data availability

All data are publicly available at http://adni.loni.usc.edu/.

Results

Cohort characteristics

One-hundred and eighty-three CU (102 Aβ− and 81 Aβ+), 61 Aβ+ MCI (including 10 individuals who progressed from CU to MCI during follow-up) and 35 Aβ+ AD participants (including 28 MCI to AD progressors) were included in the analysis. Mean follow-up time was 4.0 years (SD = 2.6). Seventy-seven participants had one Aβ PET scan, 25 had two scans, 77 had three scans and 100 had four or more scans. Two-hundred and nineteen participants had one tau PET scan, 52 had two scans and 8 had three scans. Participants had a mean age of 72 years (55–90 years), 145 (52%) were female, they had a mean of 16.5 years of education (12–20) and 114 (42%) were *APOE* ε4 carriers. Demographics are summarized in Table 1.

Disease time

Disease time was estimated for each individual (estimated previously in Li *et al.*, 2018). Disease time was centred on the average observed time of progression to an AD dementia diagnosis, making the measure interpretable at disease time = 0. The average disease time was −10, ranging from −18 to 6. The distribution of disease time by diagnosis is shown in Fig. 1 and summarized in Table 1. In 28 participants with an observed time of progression to AD, the correlation between estimated disease time and progression to AD was 0.74 ($P < 0.001$).

Regional Aβ and tau PET

Trajectories of all Aβ and tau PET ROIs are plotted against disease time in Fig. 2. Several patterns emerge, as described in more detail below. Several Aβ PET regions follow a similar pattern of high initial elevation with respect to disease time and continued increase as disease time approaches the time of an AD diagnosis. A younger sample would be required to characterize the earliest

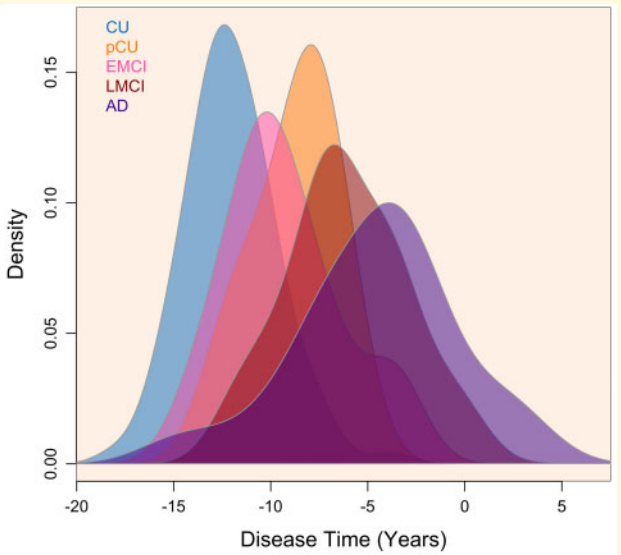

Figure 1 Disease time distributions. Distributions of baseline disease time are shown by diagnosis (pCU: CU to MCI progressors, EMCI: early MCI, LMCI: late MCI , AD: AD dementia). Disease time was re-centred so that time 0 corresponds to the mean time of progression from MCI to dementia.

Table 1 Demographics and baseline disease time

Characteristic	CU (*N* = 183)	pCU (*N* = 10)	EMCI (*N* = 30)	LMCI (*N* = 21)	AD (*N* = 35)	*P*-value
Age	71.5 (5.9)	77.0 (6.3)	69.9 (6.6)	70.5 (7.6)	74.0 (7.3)	0.01
Sex, female, *n* (%)	105 (57.4)	6 (60.0)	7 (23.3)	10 (47.6)	17 (48.6)	0.01
Education (years), *n* (%)	16.9 (2.4)	16.4 (2.8)	15.9 (2.9)	16.2 (2.6)	15.6 (2.6)	0.03
APOE ε4+, *n* (%)	59 (32.8)	5 (50.0)	20 (66.7)	13 (61.9)	17 (50.0)	<0.01
Disease time (years), *n* (%)	−11.5 (3.0)	−8.4 (1.7)	−9.3 (3.0)	−4.4 (4.0)	−3.4 (3.9)	<0.01

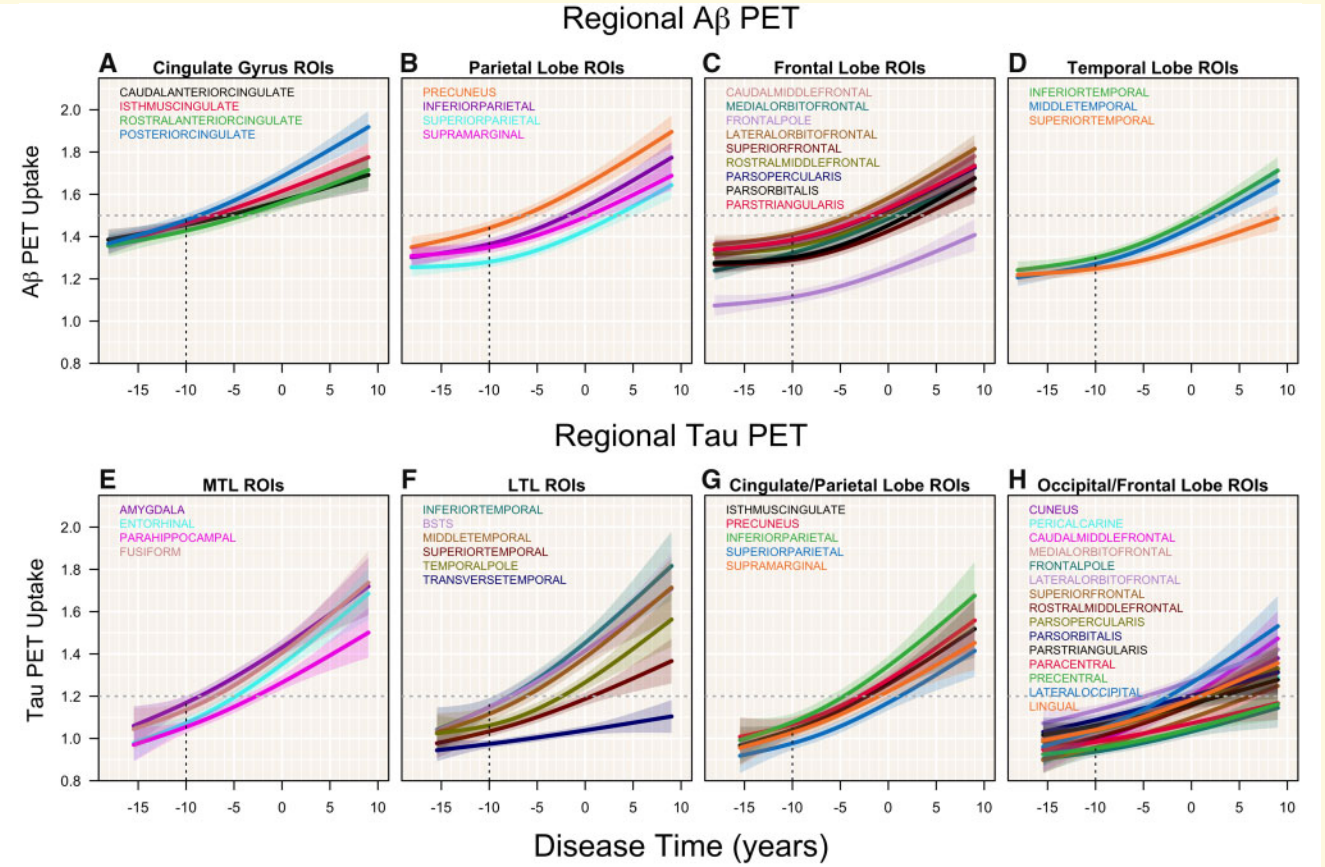

Figure 2 Aβ and tau PET ROIs. Mean uptake trajectories for Aβ and tau PET ROIs are plotted against disease time along with 95% CI depicted by the shaded regions. Aβ ROIs are shown in **A**–**D**, with a separate plot for each lobe. Tau ROIs are shown in **E**–**H**.

changes in these regions. This pattern is most noticeable in the posterior cingulate and precuneus (Fig. 2A and B). High levels of uptake are also seen initially in the isthmus cingulate, inferior parietal and lateral orbitofrontal cortex, but increased more modestly. The main tau PET region to follow this pattern of a high initial level and a steep increase was the inferior temporal lobe. The entorhinal cortex also showed a steep increase in tau uptake, as well as the fusiform, middle temporal lobe and the inferior parietal lobe. The amygdala and the BSTS showed high initial tau uptake levels, but increased modestly.

Spaghetti plots of uptake of several select ROIs are shown in Fig. 3. To more closely examine how accumulation is accelerating over the course of disease time, we plotted the first derivatives of the uptake curves against disease time in Fig. 4. These plots show the change in uptake over small advances in disease time. The posterior cingulate and isthmus cingulate show the highest initial rates of increase of Aβ uptake with respect to disease time. However, the rate of isthmus cingulate increases minimally over time. A similar pattern is seen in the caudal anterior cingulate. Large rate increases are seen in the other regions, especially in the precuneus, middle temporal lobe and the lateral orbitofrontal cortex.

Initial tau uptake slopes are steepest in the amygdala, BSTS and the inferior temporal lobe. However, the inferior temporal lobe quickly accelerates, while both the amygdala and BSTS begin to plateau. While the initial slope is more gradual in the entorhinal cortex, fusiform gyrus and middle temporal lobe, all start to accelerate, similar to the inferior temporal lobe.

Order

A positional variance diagram, depicting the order of all PET ROIs by uptake 10 years before an AD diagnosis (disease time = −10), is shown in Fig. 5. Ten years before an AD diagnosis, the Aβ PET ROIs with the highest mean uptake were the posterior cingulate, isthmus cingulate, caudal anterior cingulate and the precuneus. The tau PET ROIs with the highest mean uptake were the amygdala, inferior temporal lobe, BSTS and the fusiform gyrus. The entorhinal cortex moved to the top half of the order by 5 years before an AD diagnosis due to the slope increase over the course of disease time; otherwise, the ordering of the ROIs was stable at 15 and 5 years before an AD diagnosis (Supplementary Figs 1 and 2).

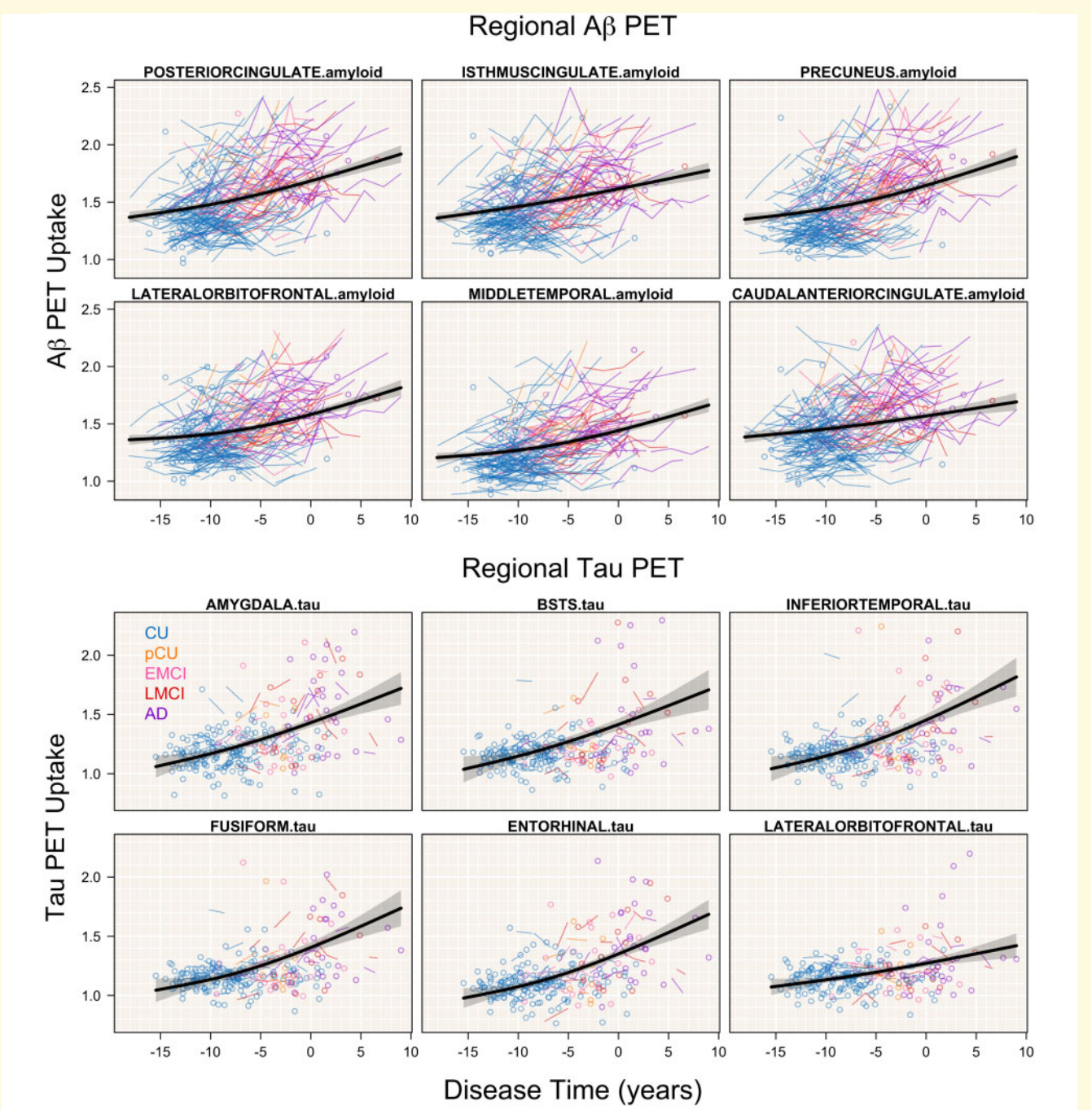

Figure 3 Select Aβ and tau PET ROIs. Mean uptake trajectories for key Aβ and tau PET ROIs are plotted against disease time along with observed subject-level data, colour coded by diagnosis. 95% CI are depicted by the shaded regions.

Early composite performance in the validation sample

To evaluate the performance of the regions selected by the LTJMM models, an outside validation sample consisting of 111 CSF Aβ− and 77 CSF Aβ+ CU participants was used. The average follow-up time of the validation sample was 2.7 years (2.8 in the Aβ− group and 2.5 in the Aβ+ group). Participants were 74 years old on average, 51% female, had an average of 16 years of education, and were 23% *APOE* ε4+.

Based on early uptake patterns, a volume-weighted average of the posterior cingulate and the precuneus were used to form the early Aβ PET composite. In Aβ− CU participants from the validation sample, there was significantly more Aβ uptake at baseline in the early composite compared to the global composite (1.25 versus 1.19, SE = 0.005, $P < 0.001$). In Aβ− CU, Aβ uptake in the

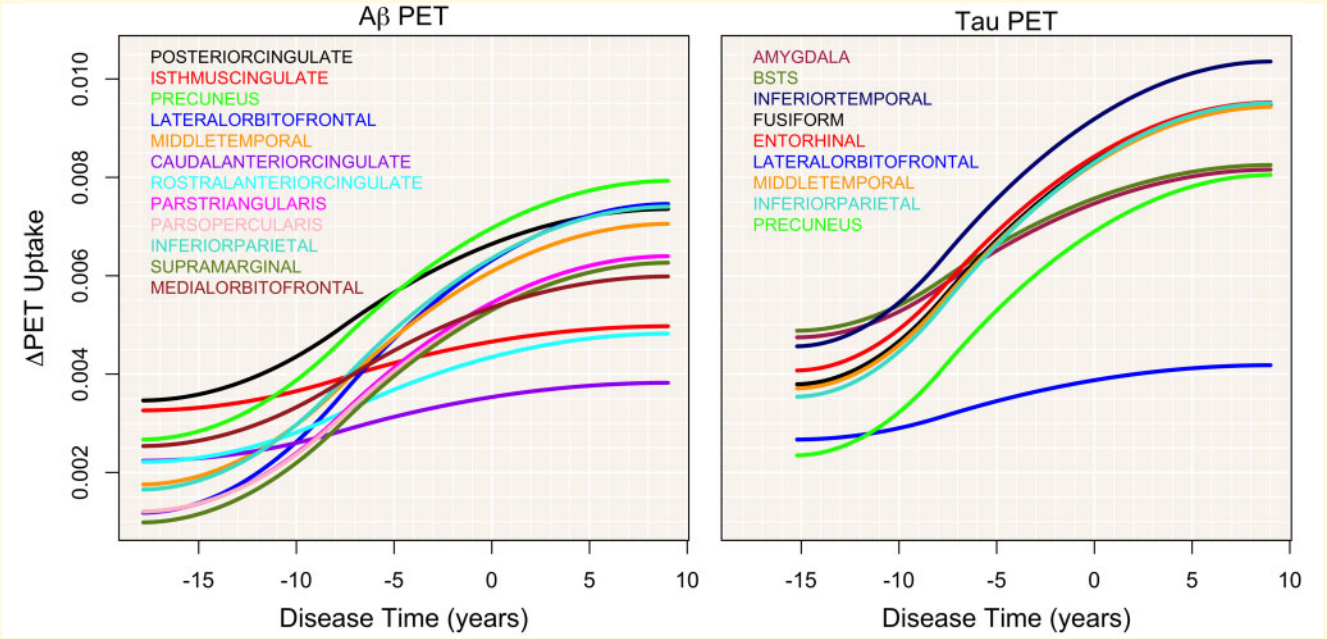

Figure 4 PET uptake change. First derivatives of the PET uptake curves are plotted against disease time for several key ROIs. Changes in the mean uptake with small increases in disease time show how the slopes of accumulation accelerate over disease time. Aβ ROIs are shown on the left and tau PET ROIs on the right.

early composite accumulated at a rate of 0.006/year [95% confidence interval (CI): 0.003–0.09, $P < 0.001$), compared to 0.003/year in the global composite (95% CI: −0.0001 to 0.006, $P = 0.06$). The accumulation rate in the early composite was more than double the rate (120% increase, $P < 0.001$) of the global composite, in the Aβ− CU participants.

In Aβ+ CU, there was significantly more uptake in the early composite at baseline compared to the global composite (1.65 versus 1.50, SE = 0.01, $P < 0.001$). The accumulation rate in the early composite was 0.013/year (95% CI: 0.003, 0.023, $P = 0.01$) and was not significantly different from the accumulation rate in the global composite, 0.012/year (95% CI: 0.003, 0.020, $P = 0.01$). Plots of baseline and change estimates are shown in Fig. 6A–D.

Power calculations for primary and secondary prevention trials

To reach 80% power in a 24-month primary prevention trial of Aβ− CU participants to detect a slowing of Aβ deposition, 233 subjects/arm would be required, using the early composite. Using the global composite with 233 subjects/arm would result in 50% power; for 80% power, 481 subjects/arm would be required.

To reach 80% power in a 24-month secondary prevention trial of Aβ+ CU participants to detect a slowing of Aβ deposition, 110 subjects/arm would be required, using the early composite. Similarly, to reach 80% power using the global composite, 106 subjects/arm would be required. Plots of power by the required sample size for hypothetical treatment trials are shown in Fig. 6E and F.

Discussion and conclusions

As the details of early biomarker changes in AD emerge, early detection and diagnosis of disease may improve by considering disease progression on its natural continuum without relying on discrete stages with artificial boundaries. By integrating biomarker and clinical data to determine each individual's location on a pathological timeline, the earliest changes in disease progression can be accurately detected and examined. In Fig. 1, the peaks of the disease time distributions align with clinical stages, although the overlap demonstrates the wide variation that is ignored when individuals are grouped discretely. As seen in Fig. 2, Aβ PET uptake levels in the posterior cingulate and precuneus start high and immediately increase with small advances in disease time, followed by multiple frontal lobe regions, especially the lateral orbitofrontal cortex, and then several parietal ROIs, with little crossing of trajectories. These regions align with multiple recent independent reports of early Aβ accumulation consistently found in the posterior cingulate, precuneus and superior frontal lobe, as well as the orbitofrontal and inferior/middle temporal lobes (Villemagne *et al.*, 2011; Vlassenko *et al.*, 2011; Mormino *et al.*, 2012; Villain

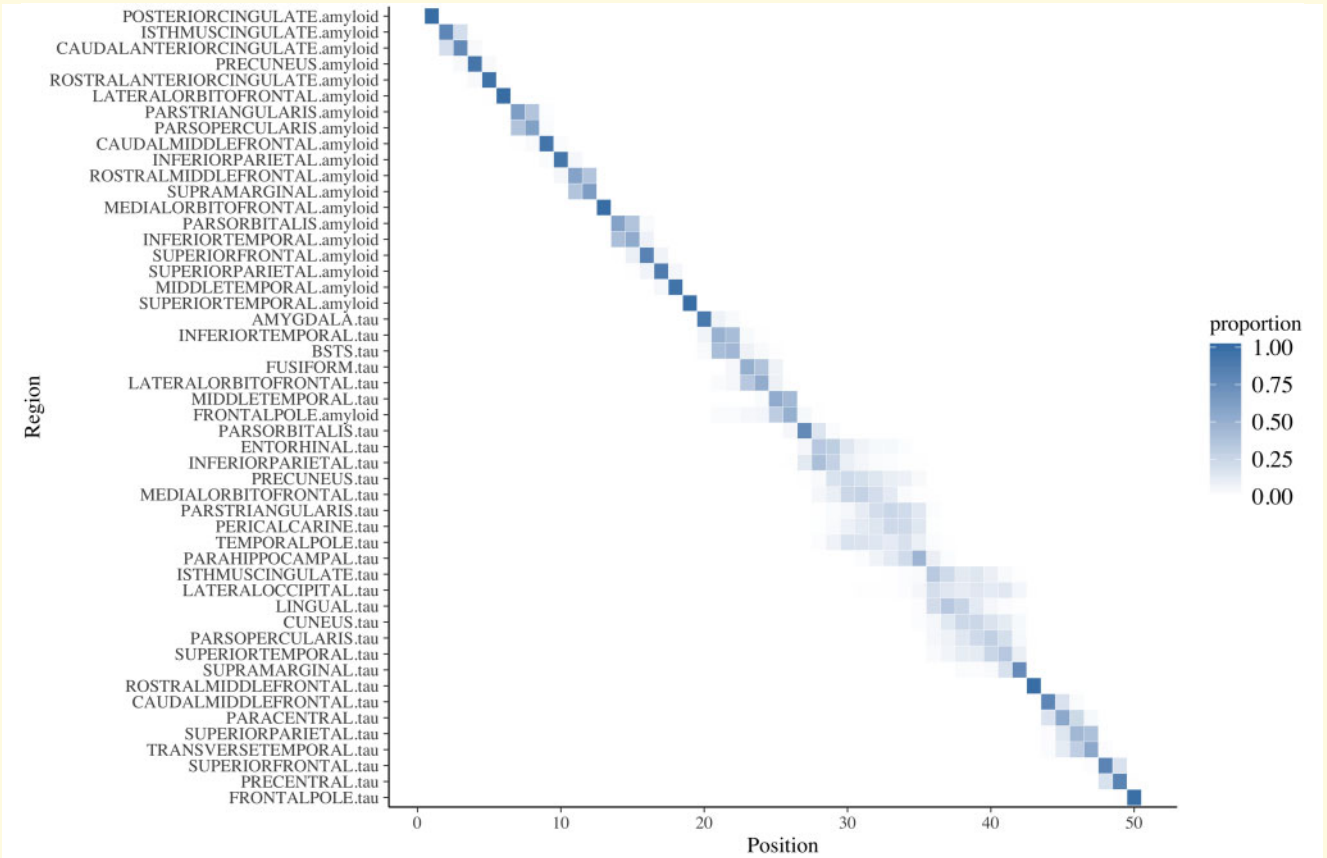

Figure 5 Positional variance diagram. The ordering of all ROIs with respect to disease time (at disease time = −10) is shown on the diagonal of the diagram. The positional variance diagram shows the proportion of 500 bootstrap samples in which a particular ROI appears in a particular position in the central ordering, ranging from 0 (white or no shading) to 1 (blue shading). ROIs are ordered by their most frequently estimated position with uncertainty captured by the transparency of the shading. Earliest accumulators are show on the top left and latest on the bottom right. Solid blue indicates increased certainty with regard to position in the order while more transparency indicates less certainty, as estimated by the bootstrap.

et al., 2012; Sojkova *et al.*, 2013; Cho *et al.*, 2016; Palmqvist *et al.*, 2017, Mattsson *et al.*, 2019c).

Similarly, early elevation and increases in tau PET uptake were found in the inferior temporal lobe, amygdala, BSTS and fusiform gyrus, and also the entorhinal cortex, inferior parietal lobe, middle temporal lobe and the precuneus. Uptake in multiple medial temporal lobe ROIs starts slightly higher and accelerates early, followed by lateral temporal and parietal lobe ROIs (Figs 2 and 3). These regions, demonstrating early elevated tau PET uptake, also coincide with several reports consistently finding elevated uptake primarily in the inferior temporal lobe, fusiform and entorhinal cortex, as well as the amygdala, parahippocampus and middle temporal lobe (Cho *et al.*, 2016; Johnson *et al.*, 2016; Schöll *et al.*, 2016; Vemuri *et al.*, 2017; Schultz *et al.*, 2018, Mattsson *et al.*, 2019b).

The order of both Aβ and tau PET ROIs remains mostly stable at different cross-sections of the disease time scale, with the exception that uptake in the entorhinal cortex accelerates quickly across disease time and moves up in the order. Several ROIs show initially elevated uptake but increase modestly with advancing disease severity. This is the case for several anterior cingulate regions in terms of Aβ uptake, including the caudal and rostral anterior cingulate. Similarly, several frontal regions, such as the lateral orbitofrontal cortex and the pars orbitalis/triangularis, show elevated tau uptake early, but do not increase at the same rate as either temporal or parietal regions, potentially due in part to the off-target binding.

The observed early pattern of uptake points to the posterior cingulate and precuneus as candidate ROIs for a targeted Aβ composite. In the validation sample, the rate of Aβ uptake in the early composite was more than twice the rate observed in the global composite, in the CSF Aβ− participants. By streamlining the commonly used global composite to include only the posterior cingulate and precuneus, the doubled rate of Aβ uptake resulted in a 60% increase in the estimated power to detect a hypothetical treatment effect in a primary prevention clinical trial. In the CSF Aβ+ participants, there was no

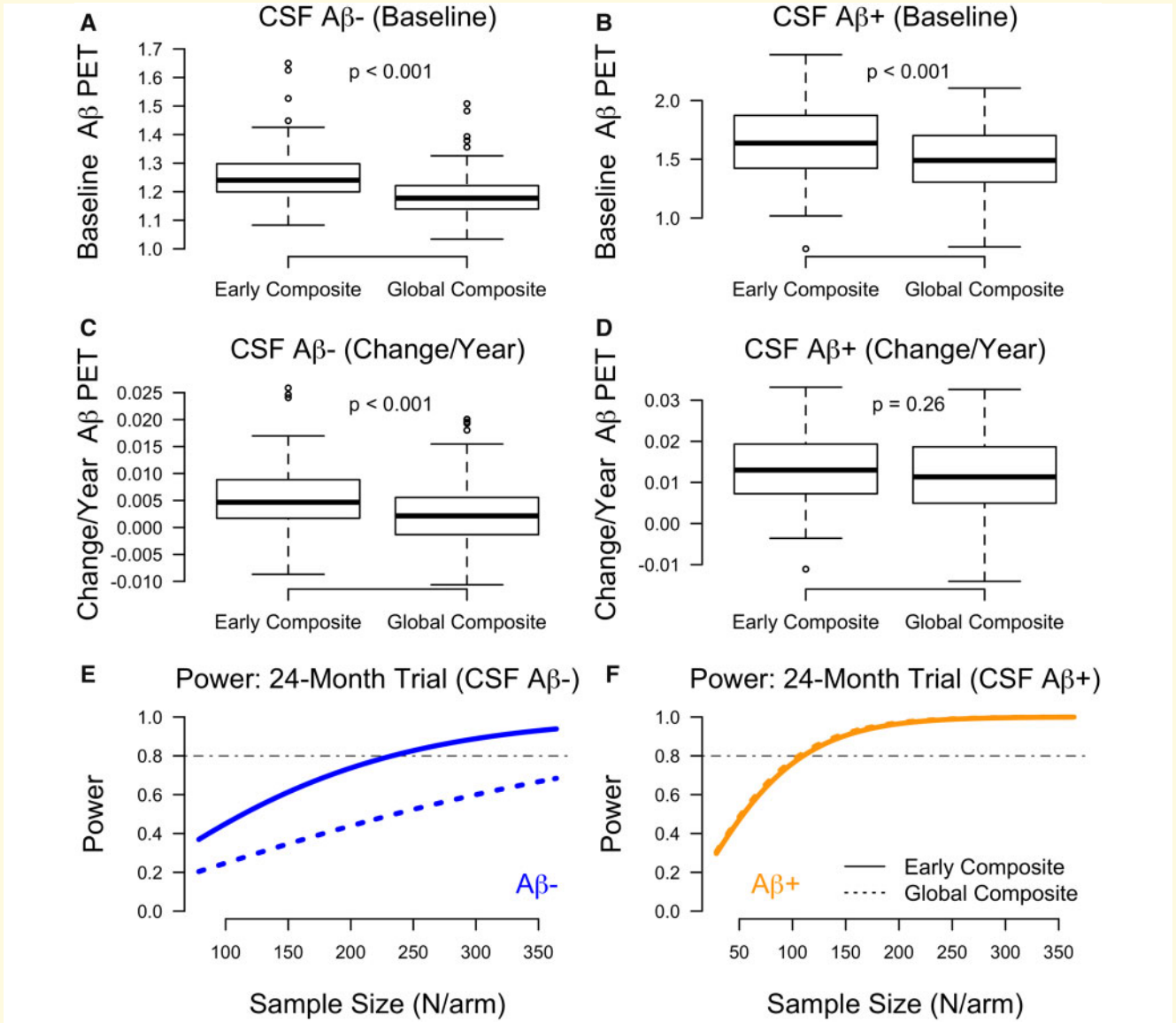

Figure 6 Early and global composite estimates and clinical trial power. Boxplots of estimates of Aβ PET uptake in early and global composites in the validation cohort. **A** and **B** show baseline estimates for CSF Aβ− and CSF Aβ+, respectively. **C** and **D** show rate estimates (Aβ PET uptake change/year) for CSF Aβ− and CSF Aβ+ participants. Plots of clinical trial power by sample size for primary prevention (Aβ−, **E**) and secondary prevention (Aβ+, **F**), for early and global composites, separately.

difference in the rate of Aβ PET uptake, suggesting that the excluded regions from the early composite are now accumulating at a similar rate observed in the early composite. Such an early composite could be used to re-examine the thresholds for Aβ-related study inclusion, especially as the field shifts to focus on secondary and primary prevention. Clinical trials of anti-Aβ treatments may benefit from the use of an early Aβ composite when estimating drug effects on Aβ changes in populations with minimal Aβ deposition and limited expected short-term accumulation.

Similarly, an early tau composite comprising the inferior temporal lobe, entorhinal cortex, amygdala, BSTS, middle temporal lobe, inferior parietal lobe and the fusiform gyrus could aid in detecting the earliest tau changes. Additional longitudinal tau PET data will be required to provide further evidence for such a composite and whether it can be optimized to correlate with early Aβ changes, neurodegeneration and the onset of cognitive symptoms.

This study is limited by its follow-up on participants younger than 65 years of age. Precise estimates of early change will require additional longitudinal follow-up focused on a younger cohort. Incorporation of emerging biomarkers such as blood-based measures of amyloid dysregulation (Nakamura *et al.*, 2018; Schindler *et al.*, 2019)

and neurodegeneration (Mattsson *et al.*, 2019a) into this effort will further clarify the course of AD.

Ordering participants on a continuous disease time scale, jointly estimated from biomarker, imaging and cognitive data, facilitates the inspection of the earliest signs of Aβ and tau pathology in the healthiest participants, informing conceptualization of the pathophysiologic processes underlying the disease. Identifying the sequence of brain regions where deposition is initiated will aid in the design of Aβ and tau composites optimized to detect and monitor disease progression facilitating the design of feasible prevention studies in AD.

Supplementary material

Supplementary material is available at *Brain Communications* online.

Acknowledgements

Data collection and sharing for this project was funded by the ADNI (National Institutes of Health Grant No. U01 AG024904). ADNI is funded by the National Institute on Aging, the National Institute of Biomedical Imaging and Bioengineering, and through generous contributions from the following: Alzheimer's Association; Alzheimer's Drug Discovery Foundation; BioClinica, Inc.; Biogen Idec, Inc.; Bristol-Myers Squibb Company; Eisai, Inc.; Elan Pharmaceuticals, Inc.; Eli Lilly and Company; F. Hoffmann-La Roche Ltd and its affiliated company Genentech, Inc.; GE Healthcare; Innogenetics, N.V.; IXICO Ltd.; Janssen Alzheimer Immunotherapy Research & Development, LLC.; Johnson & Johnson Pharmaceutical Research & Development LLC.; Medpace, Inc.; Merck & Co., Inc.; Meso Scale Diagnostics, LLC.; NeuroRx Research; Novartis Pharmaceuticals Corporation; Pfizer Inc.; Piramal Imaging; Servier; Synarc Inc.; and Takeda Pharmaceutical Company. The Canadian Institutes of Health Research is providing funds to support ADNI clinical sites in Canada. Private sector contributions are facilitated by the Foundation for the National Institutes of Health (www.fnih.org). The grantee organization is the Northern California Institute for Research and Education, and the study is coordinated by the Alzheimer's Therapeutic Research Institute at the University of Southern California, San Diego, CA. ADNI data are disseminated by the Laboratory for Neuro Imaging at the University of Southern California. Data used in the preparation of this article were obtained from the ADNI database (adni.loni.usc.edu). As such, the investigators within the ADNI contributed to the design and implementation of ADNI and/or provided data but did not participate in analysis or writing of this report. A complete listing of ADNI investigators can be found at: http://adni.loni.usc.edu/wp-content/uploads/how_to_apply/ADNI_Acknowledgement_List.pdf (also available as Supplementary material).

Funding

This research was also supported by the National Institutes of Health (NIH) Grant Nos. P30 AG010129, K01 AG030514 and R01 AG049750.

Competing interests

The authors report no competing interests.

References

Aisen PS, Cummings J, Jack CR, Morris JC, Sperling R, Frölich L, et al. On the path to 2025: understanding the Alzheimer's disease continuum. Alzheimer's Res Ther 2017; 9: 1–10.

Cho H, Choi JY, Hwang MS, Kim YJ, Lee HM, Lee HS, et al. In vivo cortical spreading pattern of tau and amyloid in the Alzheimer disease spectrum. Ann Neurol 2016; 80: 247–58.

Donohue MC, Jacqmin-Gadda H, Le Goff M, Thomas RG, Raman R, Gamst AC, et al. Estimating long-term multivariate progression from short-term data. Alzheimer's Dement 2014; 10: S400–10.

Johnson KA, Schultz A, Betensky RA, Becker JA, Sepulcre J, Rentz D, et al. Tau positron emission tomographic imaging in aging and early Alzheimer disease. Ann Neurol 2016; 79: 110–9.

Joshi AD, Pontecorvo MJ, Clark CM, Carpenter AP, Jennings DL, Mintun MA, et al. Performance characteristics of amyloid PET with florbetapir F 18 in patients with Alzheimer's disease and cognitively normal subjects. J Nucl Med 2012; 53: 378–84.

Landau SM, Mintun MA, Joshi AD, Koeppe RA, Petersen RC, Aisen PS, et al. Amyloid deposition, hypometabolism, and longitudinal cognitive decline. Ann Neurol 2012; 72: 578–86.

Li D, Iddi S, Thompson WK, Donohue MC. Bayesian latent time joint mixed effect models for multicohort longitudinal data. Stat Methods Med Res 2017; 28: 835–45.

Li D, Iddi S, Thompson WK, Rafii MS, Aisen PS, Donohue MC. Bayesian latent time joint mixed-effects model of progression in the Alzheimer's Disease Neuroimaging Initiative. Alzheimer's Dement Diagn Assess Dis Monit 2018; 10: 657–68.

Maass A, Landau S, Horng A, Lockhart SN, Rabinovici GD, Jagust WJ, et al. Comparison of multiple tau-PET measures as biomarkers in aging and Alzheimer's disease. Neuroimage 2017; 157: 448–63.

Mattsson N, Cullen NC, Andreasson U, Zetterberg H, Blennow K. Association between longitudinal plasma neurofilament light and neurodegeneration in patients with Alzheimer disease. JAMA Neurol 2019; 76: 791–9.

Mattsson N, Insel PS, Donohue M, Jögi J, Ossenkoppele R, Olsson T, et al. Predicting diagnosis and cognition with ^{18}F-AV-1451 tau PET and structural MRI in Alzheimer's disease. Alzheimer's Dement 2019; 15: 570–80.

Mattsson N, Palmqvist S, Stomrud E, Vogel J, Hansson O. Staging β-amyloid pathology with amyloid positron emission tomography. JAMA Neurol 2019; 76: 1319.

Mormino EC, Brandel MG, Madison CM, Rabinovici GD, Marks S, Baker SL, et al. Not quite PIB-positive, not quite PIB-negative: slight PIB elevations in elderly normal control subjects are biologically relevant. Neuroimage 2012; 59: 1152–60.

Nakamura A, Kaneko N, Villemagne VL, Kato T, Doecke J, Doré V, et al. High performance plasma amyloid-β biomarkers for Alzheimer's disease. Nature 2018; 554: 249–54.

Olsson A, Vanderstichele H, Andreasen N, De Meyer G, Wallin A, Holmberg B, et al. Simultaneous measurement of beta-amyloid(1-42), total tau, and phosphorylated tau (Thr181) in cerebrospinal fluid by the xMAP technology. Clin Chem 2005; 51: 336–45.

Palmqvist S, Schöll M, Strandberg O, Mattsson N, Stomrud E, Zetterberg H, et al. Earliest accumulation of β-amyloid occurs within the default-mode network and concurrently affects brain connectivity [Internet]. Nat Commun 2017; 8: 1–13.

Schindler SE, Bollinger JG, Ovod V, Mawuenyega KG, Li Y, Gordon BA, et al. High-precision plasma β-amyloid 42/40 predicts current and future brain amyloidosis. Neurology 2019; 17: e1647–e1659.

Schöll M, Lockhart SN, Schonhaut DR, O'Neil JP, Janabi M, Ossenkoppele R, et al. PET imaging of Tau deposition in the aging human brain. Neuron 2016; 89: 971–82.

Schultz SA, Gordon BA, Mishra S, Su Y, Perrin RJ, Cairns NJ, et al. Widespread distribution of tauopathy in preclinical Alzheimer's disease. Neurobiol Aging 2018; 72: 177–85.

Shaw LM, Vanderstichele H, Knapik-Czajka M, Clark CM, Aisen PS, Petersen RC, et al. Cerebrospinal fluid biomarker signature in Alzheimer's Disease Neuroimaging Initiative subjects. Ann Neurol 2009; 65: 403–13.

Sojkova J, Zhou Y, An Y, Kraut MA, Ferrucci L, Wong DF, et al. Longitudinal patterns of β-amyloid deposition in nondemented older adults. ArchNeurol 2013; 68: 644–9.

Vemuri P, Lowe VJ, Knopman DS, Senjem ML, Kemp BJ, Schwarz CG, et al. Tau-PET uptake: regional variation in average SUVR and impact of amyloid deposition. Alzheimer's Dement Diagn Assess Dis Monit 2017; 6: 21–30.

Villain N, Chételat G, Telat G, Grassiot B, Bourgeat P, Jones G, et al. Regional dynamics of amyloid-β deposition in healthy elderly, mild cognitive impairment and Alzheimer's disease: A voxelwise PiB-PET longitudinal study. Brain 2012; 135: 2126–39.

Villemagne VL, Pike KE, Chételat G, Telat G, Ellis KA, Mulligan RS, et al. Longitudinal assessment of Aβ and cognition in aging and Alzheimer disease. Ann Neurol 2011; 69: 181–92.

Vlassenko AG, Mintun MA, Xiong C, Sheline YI, Goate AM, Benzinger TLS, et al. Amyloid-beta plaque growth in cognitively normal adults: Longitudinal [^{11}C]Pittsburgh compound B data. Ann Neurol 2011; 70: 857–61.